Article:
Routledge, T.J., Lidzey, D.G. and Buckley, A.R. (2019) Ultrasonic spray coating as an approach for large-area polymer OLEDs: The influence of thin film processing and surface roughness on electrical performance. AIP Advances, 9 (1). 015330. ISSN: 2158-3226

https://doi.org/10.1063/1.5082791

AIP Advances

Ultrasonic spray coating as an approach for large-area polymer OLEDs: The influence of thin film processing and surface roughness on electrical performance

Cite as: AIP Advances 9, 015330 (2019); https://doi.org/10.1063/1.5082791
Submitted: 24 November 2018 . Accepted: 16 January 2019 . Published Online: 29 January 2019

Thomas J. Routledge, David G. Lidzey, and Alastair R. Buckley

Ultrasonic spray coating as an approach for large-area polymer OLEDs: The influence of thin film processing and surface roughness on electrical performance

Cite as: AIP Advances 9, 015330 (2019); doi: 10.1063/1.5082791
Submitted: 24 November 2018 • Accepted: 16 January 2019 •
Published Online: 29 January 2019

Thomas J. Routledge, David G. Lidzey, and Alastair R. Buckley[a)]

AFFILIATIONS

Department of Physics and Astronomy, University of Sheffield, Hicks Building, Hounsfield Road, Sheffield S3 7RH, United Kingdom

[a)]Corresponding author email: alastair.buckley@sheffield.ac.uk

ABSTRACT

In this article we present a detailed comparison of ultrasonic spray coating and spin coating for the fabrication of polymer organic light-emitting diodes (OLEDs). Single-carrier devices of hole-transporting polymer poly[(9,9-dioctylfluorenyl-2,7-diyl)-co-(4,4'(N-(4-sec-butylphenyl))) diphenylamine] (TFB) were fabricated by ultrasonic spray coating. Uniform reference devices using spin coating were also made. We have shown, across a range of device thicknesses from 37 nm to 138 nm, typical of those used in OLED hole-transport layers, that there is no statistical difference in the hole-injection efficiency between ultrasonic spray coating and spin coating. We have also demonstrated the importance of controlling the roughness of the films and we determine a threshold of 10 nm average roughness below which injection efficiency is not controlled by roughness. However, above 10 nm roughness we find a reduction in injection efficiency up to an 86 % loss in performance for roughnesses of the order of 40 % the thickness of the film. By optimising the deposition parameters, in order to allow the wet films to start to equilibrate, we find a wide processing window for smooth uniform films with excellent injection efficiency. This work reinforces the importance of ultrasonic spray coating as a potential route to high volume manufacturing of OLED based technology.

I. INTRODUCTION

Spray coating is a promising candidate for the low cost and large scale processing of polymer semiconductors for use in optoelectronic devices such as area lighting,[1] solar cells,[2,3] electrochromic devices[4,5] and transistors.[6] Ultrasonic spray coating has the benefit over other spray coating techniques, such as airbrush spraying, of increased uniformity of droplet size, leading to increased spray and film uniformity.[7,8] Ultrasonic spray coating has been used widely in polymer organic photovoltaics (OPVs), spraying single[9–11] and multilayer devices[12–15] but the use for polymer organic light-emitting diodes (OLEDs) it has so far been limited.[16,17] Gilissen et al. deposited the emissive layer of a polymer OLED via ultrasonic spray coating and achieved a power efficacy of 9.71 Lm W^{-1} compared to 12 Lm W^{-1} via spin coating.[17]

While these studies highlight the overall promise of ultrasonic spray deposition they do not elucidate potential issues or difficulties at a device structure level. In this paper we make a detailed comparison of the performance of spray versus spin coating in an exemplar device.

In ultrasonic spray coating a low concentration solution is fed onto an ultrasonic tip that vibrates at frequencies up to 35 KHz. The ultrasonic tip atomizes the solution into a fine mist of micrometre sized droplets which are then shaped and directed by a jet of gas as the spray head passes over the substrate. The individual solution droplets wet to the substrate, then spread and merge to form a complete fluid film. The film continues to flow and over time (a few seconds or more) increases in uniformity. Finally, the solvent within the film evaporates and a dry film is formed. The properties of the final film are dependent upon numerous process

parameters, such as the physical properties of the solvent–including vapour pressure, viscosity and surface energy–, solution concentration, spray head height and speed, and the substrate temperature.[8,12,18–20]

In this paper, we compare the electrical device performance of spin and spray cast films to determine the relationship between film properties and electrical properties. In order to understand spray coating the hole-injection efficiency (η) into spin cast and spray cast TFB layers of varying roughnesses was investigated across the thickness range 37-138 nm by normalizing the J-V curves for different devices via a mean-field approximation and calculating the space-charge-limited current (J_{SCLC}).

$$\eta = \frac{J_{measured}}{J_{SCLC}} \quad (1)$$

We conclude that the surface roughness plays an important role in controlling injection efficiency but that for devices fabricated using spray or spin coating, that have comparable surface roughness, no difference in charge-injection efficiency can be measured. These results suggest that there is nothing intrinsic in spray coating that limits the overall device performance. The morphology of the as-formed layer does not limit the injection efficiency and transport in our experimental devices.

II. EXPERIMENTAL

A. Device fabrication

Hole-only devices were fabricated using pre-patterned 8 pixel ITO substrates with a sheet resistance of 20 Ω square^{-1} and an rms roughness of 1.8 nm (determined by AFM) purchased from Ossila Ltd. The ITO substrates were cleaned by sonication in Hellmanex III solution, deionized water and isopropyl alcohol. Once sonicated in isopropyl alcohol the substrates were dried with nitrogen and treated with UV-Ozone for 15 minutes. Al 4083 grade PEDOT:PSS was purchased from Ossila Ltd and was filtered using a 0.45 μm PVDF mircodisc filter prior to spin coating at 5000 rpm to yield a 40 nm film. The PEDOT:PSS films were annealed on a hotplate, in air at 120 °C for 15 minutes and then cooled to room temperature prior to deposition of further layers. Poly[(9,9-dioctylfluorenyl-2,7-diyl)-co-(4,4'(N-(4-sec-butylphenyl))) diphenylamine] (TFB) was purchased from Ossila Ltd with a purity of >99 % and a molecular weight of 31,206 KDa. The spin coated TFB was cast from a toluene solution at varying concentrations in ambient conditions, from 10-30 mg ml^{-1}, and at a number of different spin speeds to obtain a range of thicknesses.

Ultrasonic spray cast TFB poly[(9,9-dioctylfluorenyl-2,7-diyl)-co-(4,4'(N-(4-sec-butylphenyl))) diphenylamine] films were deposited in ambient conditions from toluene solutions of varying concentrations (4, 6 and 8 mg ml^{-1}) using a PRISM Ultra-coat 300 system supplied by Ultrasonic systems, Inc. to give layer thicknesses of between 40 nm and 120 nm. The spray height (40 mm), base plate temperature (25 °C) and fluid pressure (50 mbar) were kept constant for each spray cast solution with the spray speed varied from 180-250 mm s^{-1} to vary the thickness of the spray cast layer. TFB has a relatively high and non-dispersive mobility as measured by time of flight technique of 0.01 cm^2 V^{-1} s^{-1}[21,22] and along with a deep HOMO of −5.3 eV,[23] excellent photochemical and thermal stability[23] makes a good test case for device process investigations. It is widely used as a copolymer constituent in light-emitting and hole-transporting layers.[24–29] It is highly soluble in aromatic solvents such as toluene, xylene, chlorobenzene and can be spray deposited from a range of these solvents. Toluene was the chosen solvent for this work as its relatively low boiling point for spray coating aids the formation of films with a range of uniformities and roughnesses.

The contacts were swabbed using toluene to pattern the device and the films were annealed at 100 °C for 10 minutes to remove any residual solvent. A bilayer top electrode of 10 nm Molybdenum(VI) oxide and 100 nm Aluminium was thermally evaporated at a vacuum pressure of 6x10^{-6} mbar through a mask to define a pixel area of 4 mm^2. After the deposition of the top electrode the devices were encapsulated in an inert atmosphere (<1 ppm H_2O and <1 ppm O_2) using UV curable epoxy and a glass slide. External electrical connection to the devices were gained via friction contacts attached to the ITO glass substrate. The top electrode being evaporated over cleared ITO tracks on the underlying substrate.

B. Device characterisation

Current-voltage sweeps were performed using a Keithley 2602 source measure unit. Thickness measurements, roughness measurements and topographical map scans were performed using a Bruker DektakXT. Map scans were replotted using Gwyddion 2.50 and statistical analysis of the data was performed using SAS Institute Inc JMP pro 13.

Thin films of TFB were deposited via both spin coating and spray coating. Thickness measurements and surface height map scans (Figure 1a) were taken of the spray cast pixels prior to the evaporation of MoO_3 and Aluminium using a Bruker DektakXT. The 1 mm by 1 mm maps are constructed from 50 line scans with resolution of 220 nm along of the line scan direction and resolution of 20000 nm in the direction orthogonal to the lines. The roughness average, R_a, is the sum of the magnitude of deviation in thickness from the mean thickness divided by the number of samples taken across the map scan. This represents the finer random irregularities of a surface rather than the larger scale thickness variations. The thickness of both spin and spray cast films as also measured by Dektak by scratching the surface of the film to the underlying substrate and scanning across the scratch. The roughness of the spin cast films was routinely measured to be less than the sensitivity of the surface profilometer (<2 nm) as such they are assumed to be perfectly uniform for space charge limited current calculations.

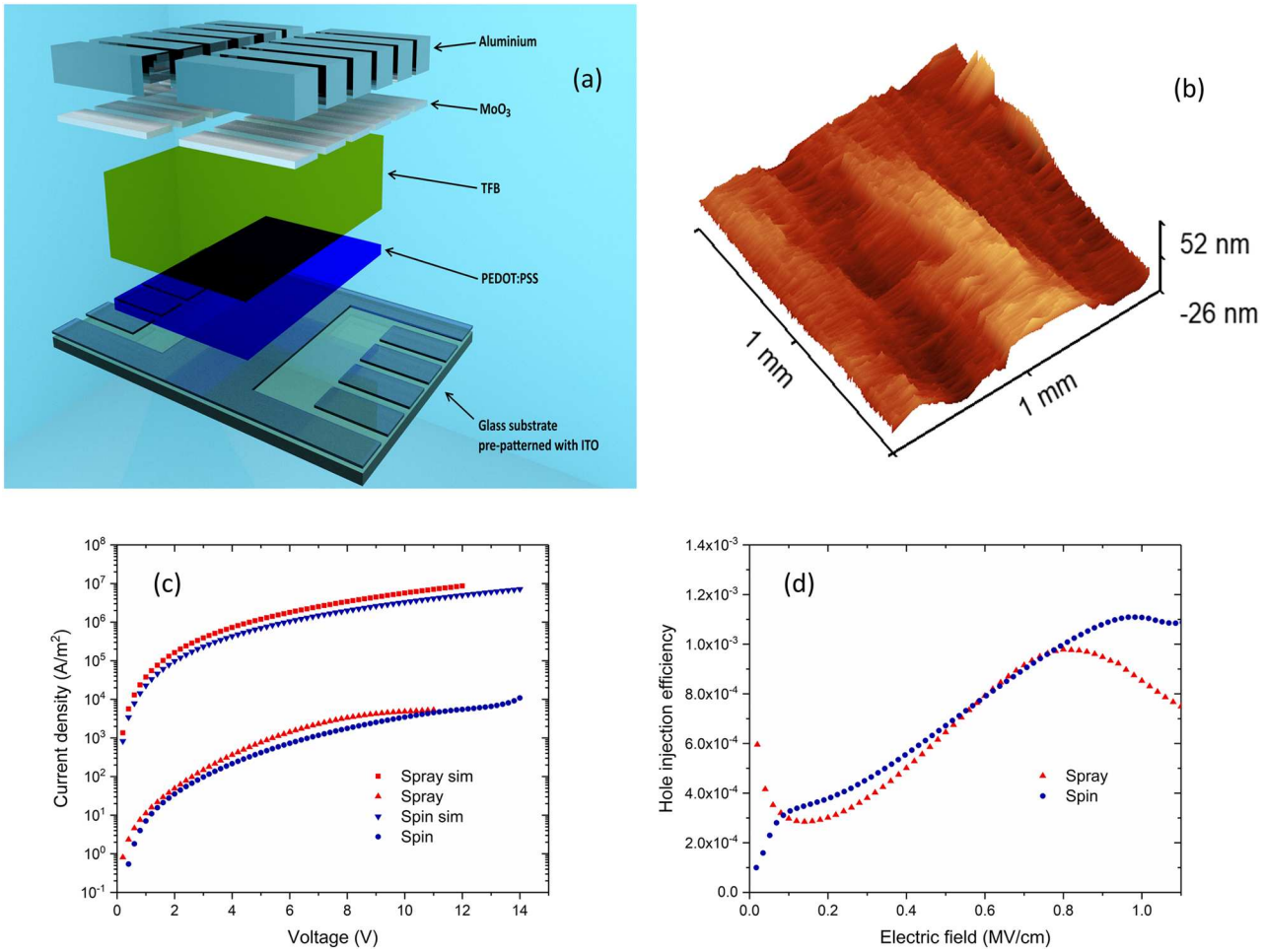

FIG. 1. (a) A 3D model of the device structure. (b) A topographical map scan of a spray cast TFB pixel (6 mg ml^{-1} S200 P4) with the mean thickness set to the measured thickness, 100 nm. (c) The current density against voltage of the space-charge-limited current simulated using (b), the measured data from the same pixel and the simulated space-charge-limited current for a uniform 116 nm thick device and the measured data from a spin cast device of the same thickness. (d) The hole-injection efficiency against electric field of the spin and spray cast pixels.

III. RESULTS AND DISCUSSION

In order to compare quantitatively the measured current-voltage characteristics of devices fabricated using spray coating and spin coating the variation in thickness between the two different processing methods needs to be normalised. In addition, the variation of thickness within pixels and the surface roughness in the spray cast devices also needs to be corrected in order that a fair comparison be made. The approach chosen follows that of Abkowitz et al.[30] and Ioannidis et al.[31] in that a charge-injection efficiency of the device is calculated by comparing the measured current to a theoretical space-charge-limited current for the thickness and material being tested. The injection efficiency has been used to probe a range of contacts as well as the ability of such contacts to inject holes into TFB.[22,32] Following Abkowitz et al.[30] we calculate a theoretical space-charge-limited current for the non-uniform devices by dividing the device into an array of parallel elements of discrete thickness and calculating a space-charge-limited current contribution from each element of the array. This is justifiable as the mean and median thickness variation between neighbouring array elements are less than 1 nm (further discussion in the supplementary), as such the films are locally smooth but globally rough across the device.

The theoretical space-charge-limited current is calculated using a modified Mott-Gurney relationship[33] with a Poole-Frenkel field dependent mobility,[34] $j = \frac{9}{8}\varepsilon_0\varepsilon_r\mu\frac{\bar{E}^2}{L}exp\left(\gamma\sqrt{\bar{E}}\right)$. Where ε_r is the relative permittivity, μ is the bulk mobility, L is the layer thickness, γ is the field dependent factor and $\bar{E}$ is the mean electric field. A mean-field approximation is used to simplify the calculation for different thickness elements in the intra-device array. This approximation is shown to be valid[35–38] and leads to typical under estimation in

zero-field mobility and the γ factor of 2 % and 15 % respectively[39] and an error in calculated j of 10 %. For TFB the bulk mobility is taken as 0.01 $cm^2\ V^{-1}\ s^{-1}$,[21] the relative permittivity $\varepsilon_r \sim 3$[40] and field dependent factor $\gamma = 5.86 \times 10^{-4}\ (cm\ V^{-1})^{0.5}$.[22]

The theoretical space-charge-limited current values were compared to the measured current density values of the same pixels (Figure 1b) to show the variation of hole-injection efficiency against electric field (Figure 1c). The hole-injection efficiency at a fixed electric field (1 MV cm^{-1}) was used for direct comparison of pixels of different thicknesses and deposition techniques. In this paper we combine electrical measurements, topographical map scans and theoretical models to determine the hole-injection efficiency of MoO_3 into TFB films. The hole-injection efficiency is used to probe the charge transport in TFB films across a range of thickness equivalent to those optimal for OLEDs, allowing us to compare the deposition techniques of ultrasonic spray coating and spin coating for the fabrication of OLEDs.

Figure 2 shows the variation of injection efficiency from MoO_3 into a range of different thicknesses of TFB deposited via spin coating and ultrasonic spray coating. Figure 1(a) shows a schematic of the device structure, consisting of ITO/PEDOT:PSS/TFB/MoO_3/Aluminium. The thickness and deposition method of the PEDOT:PSS (40 nm), MoO_3 (10 nm) and Aluminium (100 nm) are consistent for all devices. The thickness ranges covered by the two deposition techniques of TFB overlap allowing for the direct comparison of injection efficiency and thus the performance of spin and spray cast devices.

Looking first at the spin cast TFB devices (Figure 2a) we see that the injection efficiency increases with thickness (within this range). The injection efficiency has been shown to vary due to the material used for injection,[22] the thickness of that layer[41] and the applied electric field.[22] In this work the injection material and thickness have been kept constant and the injection efficiencies were all measured at the same electric field strength. The mobility of materials with similar properties to TFB have been studied in literature; Ji et al. measured the mobility of pi-conjugated polymer P3HT in organic thin film transistors and demonstrated that mobility increases with thickness within the device thickness region (0-200 nm),[42] Chu et al.[35,43] demonstrated the mobility of hole-transporting small molecule NPB increases with thickness in an similar range as did Xu et al. who also demonstrated the same trend for hole-transporting small molecule TPD.[44] It can then be inferred that the increase in injection efficiency is due to an increase in the effective mobility of the TFB film toward the bulk mobility.[45]

To understand the microscopic structure and the effect on the charge injection and transport within a film it is often assumed that a film is made up of the substrate interface, the surface interface and the bulk of the film.[44,46–49] In this work we focus on two regions; the interfacial region at the surface of the TFB where the holes are injected from the MoO_3, and the bulk of the TFB. In a uniform thick film the interfacial region will be small compared to the film thickness and the charge dynamics of the film will be dominated by that of the bulk TFB, in thinner films the interfacial region thickness will be a larger proportion of the thickness of the film as a whole and such will play a larger part in charge dynamics of the film. The influence of the interfacial regions on the charge dynamics of the film has been studied by Baldo et al.[49] for electron transport in Alq_3, by Chu et al.[35,43] for hole transport in NPB, Xu et al.[44] for hole transport in TPD and by Harding et al. for interlayers of TFB.[50] These works suggest that there are trap states in the injection interfacial region which result from dipole interactions between MoO_3 and TFB, changes in the polymer chain conformation or a combination of both. The disorder in the local dipole fields in the interfacial region cause a broadening of the manifold of states involved in hopping transport as such

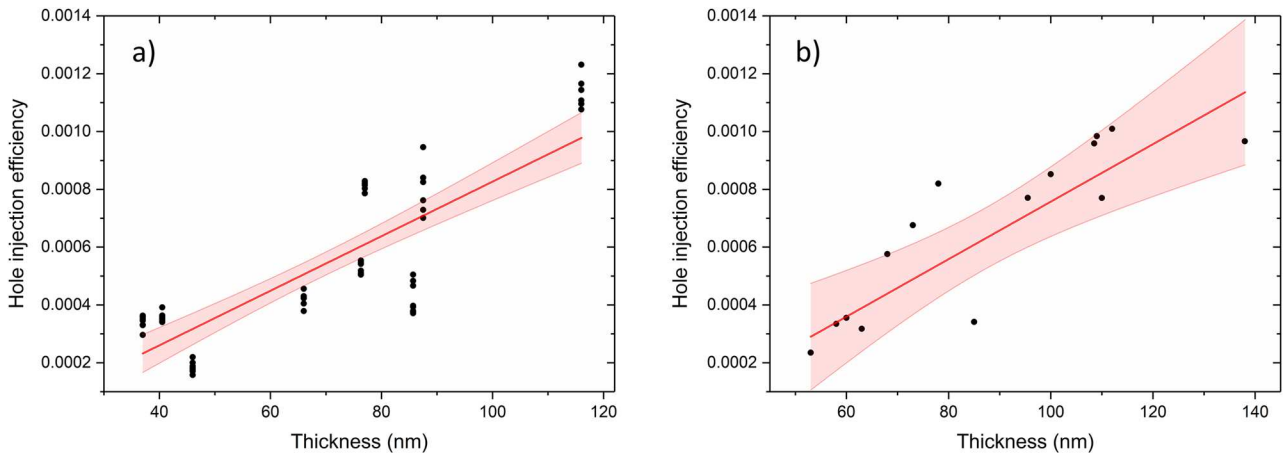

FIG. 2. (a) The injection efficiency at 1 MV cm^{-1} against thickness for the spin cast pixels, a liner regression has been fitted and the shaded region demonstrates the 95 % confidence interval. The linear regression fit has a P-value of <0.0001 and an R-squared adjusted value of 0.66 (b) The injection efficiency at 1 MV cm^{-1} against thickness for the spray cast pixels, a linear regression has been fitted and the shaded region demonstrates the 95 % confidence interval. The linear regression fit has a P-value of 0.0003 and an R-squared adjusted value of 0.59.

TABLE I. Comparing the key fit parameters; fit gradient, fit intercept, P value and R-square adjusted for the spin cast and spray cast models dependent on thickness, and the spray cast model dependent on thickness and roughness.

	Spin cast fit	Spray cast single parameter fit	Spray cast two parameter fit
R-sq. adjusted	0.66	0.59	0.91
Fit Gradient	$(9.4 \pm 0.8) \times 10^{-6}$	$(9.9 \pm 2.1) \times 10^{-6}$	$(9.4 \pm 1.0) \times 10^{-6}$
Fit intercept	$(-1.2 \pm 0.6) \times 10^{-4}$	$(-2.4 \pm 1.9) \times 10^{-4}$	$(-1.9 \pm 0.8) \times 10^{-4}$
Model P value	<0.0001*	0.0003	<0.0001*

lowering the effective mobility. Changes in the conformation of polymer chains can also increase the intersite hopping distance for holes, reducing the hopping rate and thus lowering the effective mobility.

Figure 2b shows the injection efficiency of spray cast TFB devices increases with thickness like that of spin cast devices. A linear regression fit was applied to the spin cast and spray cast data, the gradients and intercepts of the spin cast and spray cast models agree within errors (Table I), thus suggesting that device performance of spray cast devices is statistically equivalent to spin cast devices.

Since the roughness of the surface of spin cast TFB is too low to be reliably measured by the technique used in this experiment (<2 nm) the spin cast pixels were assumed to be uniform with no significant roughness. The process of forming a film via spray coating can lead to non-uniform thickness up to 52 nm from the mean (Figure 1b). Using map scans the thickness variation between array elements across spray cast devices were measured and taken into account in the initial spray cast linear regression fit, but the roughness of these devices was not accounted for. Figure 3 shows the injection efficiency residuals from spray cast linear regression fit verses thickness, plotted against the roughness average. The residual in this case is the difference between the measured value of injection efficiency and the predicted value of injection efficiency from the linear regression fit based on thickness variation. The injection efficiency residuals decrease with increasing roughness, and above a Ra of around 10 nm the residuals become negative. The R-square adjusted value for this fit is 0.79 thus roughness has a significant effect on the injection efficiency. Rougher films, as-prepared by higher concentration formulations and faster pass speeds, lead to lower overall charge-injection efficiency. These films dry faster on the substrate, and within the film, the surface dries fastest of all. The consequence is that the surfaces of these rough films have less time to equilibrate in terms of molecular conformation and mixing. We believe this leads to a lock-in of a non-equilibrium conformation within the film surface with a higher dispersion in the distribution of energy states that form the hole-transport manifold. This in turn leads to lower effective mobility and a lower hole-injection efficiency for the rougher films.

Figure 4 shows the measured hole-injection efficiency of the spray cast devices plotted against the injection efficiency predicted by the linear regression fit incorporating thickness and roughness. The measured and predicted data

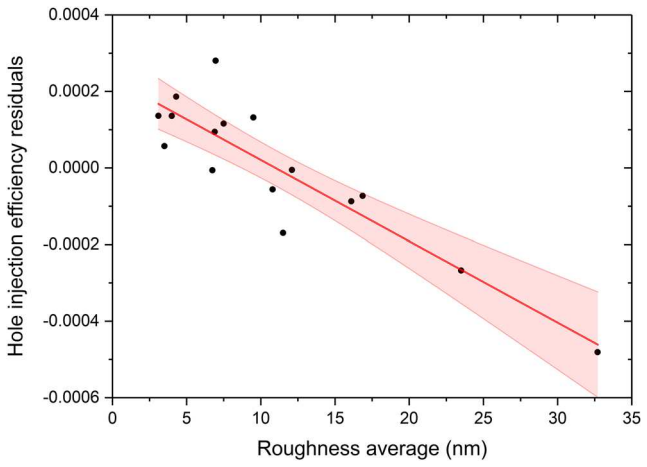

FIG. 3. The injection efficiency residual, the calculated hole injection efficiency minus the hole injection efficiency predicted by the initial spray cast linear regression fit, at 1 MV cm^{-1} against the roughness average (Ra) of the spray cast device pixels. The linear regression fit has a P-value <0.0001 and R-squared adjusted 0.79, the shaded region demonstrates the 95 % confidence interval.

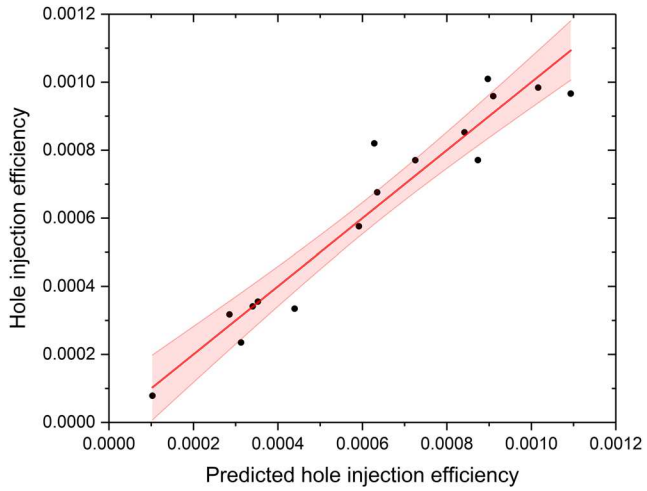

FIG. 4. The calculated injection efficiency against the predicted injection efficiency by the linear regression fit based on the variation due to thickness and the roughness of the spray-cast TFB layer (at 1 MV cm^{-1}). The shaded region demonstrates the 95 % confidence interval from the fit.

are strongly correlated and the confidence interval is very narrow.

Table I compares the spin cast, single parameter spray cast and two parameter spray cast linear regression fits for hole-injection efficiency plotted against thickness. The errors in the gradient and intercept are reduced when going from the single to the two parameter spray cast models. The gradient and intercept values of the two parameter spray cast model are closer to the values of the spin cast model than those of the single parameter spray cast model and they agree within errors. The p value of the two parameter spray-cast model compared to the single parameter model has decreased from 0.0003 to <0.0001 as such the two parameter spray cast model p value is highly significant as is found in the spin cast model. This suggests that if the ultrasonic spray coating process is optimised to minimize roughness then overall device performance of OLEDs deposited via ultrasonic spray coating can equal those fabricated by spin coating.

IV. CONCLUSIONS

We have compared the injection efficiency of holes into films of poly[(9,9-dioctylfluorenyl-2,7-diyl)-co-(4,4'(N-(4-sec-butylphenyl))) diphenylamine], cast by ultrasonic spray coating with those cast by spin coating. We have shown, across a range of thicknesses typical of those used in OLEDs, that there is no intrinsic difference in the injection efficiency between ultrasonic spray coating and spin coating. This reinforces the importance of spray coating as a potential route to high volume manufacturing of OLED based technology. We have also demonstrated the importance of controlling the roughness of the films and we determine a threshold of 10 nm average roughness below which injection efficiency is not controlled by roughness. However, above 10 nm roughness we find a reduction in injection efficiency up to an 86 % loss in performance for roughnesses of the order of 40 % of the thickness of the film. However, the process window for achieving comparable spin and spray cast hole-injection performance is wide with spray cast films with Ra < 10 nm being easily achieved by control of drying time through solvent choice, substrate temperature, formulation concentration and pass speed.

SUPPLEMENTARY MATERIAL

See supplementary material for justification of dividing the device into an array of parallel elements and calculating a current density for each element separately as well as plots of the residuals of the linear regression fits for the models plotted in Figures (2)a, (2)b and 4.

ACKNOWLEDGMENTS

We thank financial support from EPSRC via grants 1572317 "Advanced materials and processing for OLEDs", EP/M025020/1 and EP/M014797/1. We thank Prof. Richard Jones and Dr. Andrew Parnell for their contributions towards discussions around this work.

REFERENCES

[1]A. Sandström, A. Asadpoordarvish, J. Enevold, and L. Edman, Adv. Mater. **26**, 4975 (2014).
[2]C. N. Hoth, R. Steim, P. Schilinsky, S. A. Choulis, S. F. Tedde, O. Hayden, and C. J. Brabec, Org. Electron. Physics, Mater. Appl. **10**, 587 (2009).
[3]J. W. Kang, Y. J. Kang, S. Jung, M. Song, D. G. Kim, C. S. Kim, and S. H. Kim, Sol. Energy Mater. Sol. Cells **103**, 76 (2012).
[4]P. Shi, C. M. Amb, E. P. Knott, E. J. Thompson, D. Y. Liu, J. Mei, A. L. Dyer, and J. R. Reynolds, Adv. Mater. **22**, 4949 (2010).
[5]C. M. Amb, P. M. Beaujuge, and J. R. Reynolds, Adv. Mater. **22**, 724 (2010).
[6]B. S. Hunter, J. W. Ward, M. M. Payne, J. E. Anthony, O. D. Jurchescu, and D. Thomas, **223304**, 1 (2015).
[7]R. Engle and Sono-Tek Present. 15th Int. Coat. Sci. Technol. Symp. (2010).
[8]M. Majumder, C. Rendall, M. Li, N. Behabtu, J. A. Eukel, R. H. Hauge, H. K. Schmidt, and M. Pasquali, Chem. Eng. Sci. **65**, 2000 (2010).
[9]K. X. Steirer, M. O. Reese, B. L. Rupert, N. Kopidakis, D. C. Olson, R. T. Collins, and D. S. Ginley, Sol. Energy Mater. Sol. Cells **93**, 447 (2009).
[10]J. G. Tait, B. P. Rand, and P. Heremans, Org. Electron. Physics, Mater. Appl. **14**, 1002 (2013).
[11]T. Wang, N. W. Scarratt, H. Yi, A. D. F. Dunbar, A. J. Pearson, D. C. Watters, T. S. Glen, A. C. Brook, J. Kingsley, A. R. Buckley, M. W. A. Skoda, A. M. Donald, R. A. L. Jones, A. Iraqi, and D. G. Lidzey, Adv. Energy Mater. **3**, 505 (2013).
[12]C. Girotto, D. Moia, B. P. Rand, and P. Heremans, Adv. Funct. Mater. **21**, 64 (2011).
[13]Y. Zhang, J. Griffin, N. W. Scarratt, T. Wang, and D. G. Lidzey, Prog. Photovolt Res. Appl. **24**, 275 (2016).
[14]Y. Zhang, N. W. Scarratt, T. Wang, and D. G. Lidzey, Vacuum **139**, 154 (2017).
[15]N. W. Scarratt, J. Griffin, T. Wang, Y. Zhang, H. Yi, A. Iraqi, and D. G. Lidzey, APL Mater. **3**, 126108 (2015).
[16]K. Gilissen, J. Stryckers, J. Manca, and W. Deferme, Proc. SPIE - Int. Soc. Opt. Eng. **9183**, 918311 (2014).
[17]K. Gilissen, J. Stryckers, P. Verstappen, J. Drijkoningen, G. H. L. Heintges, L. Lutsen, J. Manca, W. Maes, and W. Deferme, Org. Electron. Physics, Mater. Appl. **20**, 31 (2015).
[18]M. Eslamian, Coatings **4**, 60 (2014).
[19]J. E. Bishop, D. K. Mohamad, M. Wong-Stringer, A. Smith, and D. G. Lidzey, Sci. Rep. **7**, 7962 (2017).
[20]A. T. Barrows, A. J. Pearson, C. K. Kwak, A. D. F. Dunbar, A. R. Buckley, and D. G. Lidzey, Energy Environ. Sci. **7**, 2944 (2014).
[21]H. H. Fong, A. Papadimitratos, and G. G. Malliaras, Appl. Phys. Lett. **89**, 172116 (2006).
[22]H. H. Fong, A. Papadimitratos, J. Hwang, A. Kahn, and G. G. Malliaras, Adv. Funct. Mater. **19**, 304 (2009).
[23]B. M. Redecker, D. D. C. Bradley, M. Inbasekaran, W. W. Wu, and E. P. Woo, Adv. Funct. Mater. **11**, 241 (1999).
[24]T. Chiba, Y. J. Pu, M. Hirasawa, A. Masuhara, H. Sasabe, and J. Kido, ACS Appl. Mater. Interfaces **4**, 6104 (2012).
[25]Y. Chen, Y. Xia, G. M. Smith, H. Sun, D. Yang, D. Ma, Y. Li, W. Huang, and D. L. Carroll, Adv. Funct. Mater. **24**, 2677 (2014).
[26]S. A. Choulis, V. Choong, M. K. Mathai, F. So, S. A. Choulis, V. Choong, M. K. Mathai, and F. So, **113503**, 2003 (2005).
[27]S.-R. Tseng, S.-Y. Li, H.-F. Meng, Y.-H. Yu, C.-M. Yang, H.-H. Liao, S.-F. Horng, and C.-S. Hsu, Org. Electron. **9**, 279 (2008).
[28]S.-R. Tseng, S. Y. Li, H. F. Meng, Y. H. Yu, C. M. Yang, H. H. Liao, S. F. Horng, and C. S. Hsu, J. Appl. Phys. **101**, 084510 (2007).
[29]J. Wang, N. Wang, Y. Jin, J. Si, Z. K. Tan, H. Du, L. Cheng, X. Dai, S. Bai, H. He, Z. Ye, M. L. Lai, R. H. Friend, and W. Huang, Adv. Mater. **27**, 2311 (2015).
[30]M. Abkowitz, J. S. Facci, and J. Rehm, J. Appl. Phys. **83**, 2670 (1998).
[31]A. Ioannidis, J. S. Facci, and M. A. Abkowitz, J. Appl. Phys. **84**, 1439 (1998).
[32]Y. Shen, A. R. Hosseini, M. H. Wong, and G. G. Malliaras, ChemPhysChem **5**, 16 (2004).
[33]N. F. Mott and R. W. Gurney, *Electronic Processes in Ionic Crystals* (Clarendon Press, Oxford, 1940).

[34]E. H. Sondheimer, Adv. Phys. **1**, 1 (1952).
[35]T.-Y. Chu and O.-K. Song, Appl. Phys. Lett. **90**, 203512 (2007).
[36]M. Giulianini, E. R. Waclawik, J. M. Bell, and N. Motta, Appl. Phys. Lett. **94**, 3 (2009).
[37]O. G. Reid, K. Munechika, and D. S. Ginger, Nano Lett. **8**, 1602 (2008).
[38]A. Pitarch, K. Meerholz, and D. Hertel, Phys. Status Solidi Basic Res. **245**, 814 (2008).
[39]A. R. Buckley, Synth. Met. **160**, 540 (2010).
[40]P. Blom, M. de Jong, and M. van Munster, Phys. Rev. B - Condens. Matter Mater. Phys. **55**, R656 (1997).
[41]A. Buckley, D. Pickup, C. Yates, Y. Zhao, and D. Lidzey, J. Appl. Phys. **109**, 1 (2011).
[42]H. Jia, S. Gowrisanker, G. K. Pant, R. M. Wallace, and B. E. Gnade, J. Vac. Sci. Technol. A Vacuum, Surfaces, Film. **24**, 1228 (2006).
[43]T. Y. Chu and O. K. Song, J. Appl. Phys. **104** (2008).
[44]H. Xu, W.-J. Zhai, C. Tang, S.-Y. Qiu, R.-L. Liu, Z. Rong, Z.-Q. Pang, B. Jiang, J. Xiao, C. Zhong, B.-X. Mi, Q.-L. Fan, and W. Huang, J. Phys. Chem. C **120**, 17184 (2016).
[45]Y. Shen, M. W. Klein, D. B. Jacobs, J. Campbell Scott, and G. G. Malliaras, Phys. Rev. Lett. **86**, 3867 (2001).
[46]T. Wang, A. J. Pearson, A. D. F. Dunbar, P. A. Staniec, D. C. Watters, D. Coles, H. Yi, A. Iraqi, D. G. Lidzey, and R. A. L. Jones, Eur. Phys. J. E **35**, 2 (2012).
[47]D. Liu, R. Osuna Orozco, and T. Wang, Phys. Rev. E **88**, 022601 (2013).
[48]R. Noriega, J. Rivnay, K. Vandewal, F. P. V Koch, N. Stingelin, P. Smith, M. F. Toney, and A. Salleo, Nat. Mater. **12**, 1038 (2013).
[49]M. A. Baldo and S. R. Forrest, Phys. Rev. B - Condens. Matter Mater. Phys. **64**, 1 (2001).
[50]M. J. Harding, D. Poplavskyy, V. E. Choong, F. So, and A. J. Campbell, Adv. Funct. Mater. **20**, 119 (2010).